Int. J. Electrochem. Sci., 16 **(2021)** Article ID: 210553, doi: 10.20964/2021.05.62

International Journal of
ELECTROCHEMICAL
SCIENCE
www.electrochemsci.org

Study on Ni/MH Composite Plating and Its Performance for Hydrogen Evolution Reaction

Shouguang Yao[1,*], *Hao Xu*[1,2,3], *Min Xiao*[1], *Jie Cheng*[2,3], *Yusheng Yang*[2,3]

[1] School of Energy and Power Engineering, Jiangsu University of Science and Technology, Zhenjiang, Jiangsu 212003, China
[2] Zhangjiagang Smartgrid Fanghua electrical energy storage research institute Co. Ltd., Zhangjiagang 215600, China
[3] Chilwee Power Co., Ltd., Huzhou 313100, China
[*]E-mail: zjyaosg@126.com

Received: 25 January 2021 / *Accepted:* 11 March 2021 / *Published:* 31 March 2021

In order to improve the hydrogen evolution stability of nickel electrodes, this paper prepares a composite nickel-plated/hydrogen storage alloy (Ni/MH) electrode and investigates its hydrogen evolution performance in alkaline aqueous solutions. Characterization results such as scanning electron microscopy (SEM), X-ray diffraction (XRD) and energy dispersive spectrometer (EDS) indicate that the hydrogen storage alloy particles have been uniformly deposited inside and on the surface of the nickel plating, and that pores exist on the electrode surface. The linear sweep voltammetry (LSV) at room temperature shows that the overpotential of the Ni/MH composite electrode is 196 mV when the current density reaches 50 $mA \cdot cm^{-2}$ and 231 mV when the current density reaches 100 $mA \cdot cm^{-2}$. The tafel slope of 100 $mV \cdot dec^{-1}$, which performs much better than nickel-plated electrodes. Chronopotentiometry (CP) showed that the potential response of the Ni/MH composite electrode was very stable and comparable to that of the Pt electrode, while the Ni electrode polarization continued to increase. Electrochemical impedance spectroscopy (EIS) tests confirmed that the Ni/MH composite electrode had a low charge transfer resistance. In summary, the results show that composite plating with hydrogen storage alloy significantly improves the hydrogen evolution catalytic performance of nickel electrodes and has a broad application prospect.

Keywords: Composite nickel/hydrogen storage alloy electrode; Catalytic activity of hydrogen evolution; Stability; Overpotential

1. INTRODUCTION

With the gradual depletion of fossil energy sources, the search for alternative new energy sources has become an urgent task. Hydrogen is an abundant renewable energy source with a high calorific value

and is therefore widely considered as an important alternative to fossil energy sources [1, 2]. Hydrogen production by electrolysis of water is a sustainable, safe and green way of hydrogen production and produces hydrogen with high purity [3]. At present, hydrogen production by electrolysis of alkaline solution is a more mature method for hydrogen production in industry, however, energy consumption problems, high overpotential of cathode, catalyst activity and durability have been affecting the alkaline electrolytic water production industry. Although Pt-based electrodes have high catalytic activity and stability, their high cost and resource scarcity limit their application in hydrogen production [4]. Ni-based alloys are recognized as a non-noble metal material with high catalytic activity, such as binary alloys Ni-Mo and Ni-Co [5], and ternary alloys Ni-Mo-Co and Ni-Mo-Fe [6] are formed by introducing other elements into nickel to form alloys that change the adsorption/desorption capacity on adjacent Ni atoms to promote the catalytic process of Ni. Ni-based alloys have a low oxidation resistance, the polarization becomes continuously larger during hydrogen evolution, and they are more prone to oxidative deactivation after power failure. For example, the electrochemical stability of Ni-Mo alloys is poor due to solution erosion and other reasons, and the hydrogen evolution reaction activity degrades quickly in use [7].

Lanthanum-nickel alloys ($LaNi_5$) have a $CaCu_5$-type hexagonal structure and are widely used as hydrogen storage alloys due to the presence of many interstitial spaces in their lattice structure capable of absorbing large amounts of hydrogen [8]. In recent years, the use of $LaNi_5$ as a hydrogen evolution cathode for electrolytic water has attracted the attention of others. Zhang's group [9] and Song's group [10] used composite electrodeposition technique to embed $LaNi_5$ solid particles into Ni metal plating to form Ni/$LaNi_5$ composite plating, and this composite electrodeposition method improved the specific surface area and catalytic activity of the electrodes. Han's group [11] prepared $LaNi_5$ plating using molten salt electrolysis followed by electrodeposition of Ni-S alloy plating on the surface to form a dual plating structure, and electrochemical tests showed that the composite electrode had high electrochemical activity. However, the constant adsorption/desorption of hydrogen by $LaNi_5$ causes the $LaNi_5$ alloy volume to alternate between expansion and contraction resulting in hydrogen embrittlement chalking [12, 13], making the catalysts unusable for long periods of time. In contrast, AB_5-type alloys doped with multiple elements can stabilize the lattice structure of the alloy by reducing the lattice volume expansion rate during hydrogenation and suppressing the atomic migration during cycling [14], thus improving stability during hydrogen evolution.

In this paper, with the aim of improving the catalytic activity and stability of hydrogen evolution, a composite electrode (Ni/MH) with high catalytic activity and high stability was made by composite electrodeposition of the multi-metal hydrogen storage alloy $MmNi_{4.05}Co_{0.45}Mn_{0.38}Al_{0.3}$ into the Ni metal plating layer. Scanning electron microscopy (SEM), X-ray diffraction (XRD) and energy spectrometry (EDS) were used to determine the plating morphology, structure and content of each element. After that, electrochemical methods such as polarization curves (LSV), chronopotentiometry (CP) and electrochemical impedance spectroscopy (EIS) were used to evaluate the catalytic activity and stability of the composite coatings for hydrogen evolution.

2. EXPERIMENTAL SECTION

2.1. Reagents and instruments

Commercially available hydrogen storage alloy (MH) powder (model MC-03, $MmNi_{4.05}Co_{0.45}Mn_{0.38}Al_{0.3}$, average particle size: 50 μm, Mm is a mixture of La and Ce rare earths with La content of 22.5 wt% and Ce content of 9.7 wt%, Xiamen Tungsten Industry Co.), Boric acid (H_3BO_4, analytical purity, Jiangxi Wanchang Sanitary Products Co., Ltd.), hydrochloric acid (HCl, 37% vol analytical purity, Huadong Pharmaceutical Co., Ltd.), acetone (C_3H_6O, analytical purity, Jiangsu Yong Hua Chemical Technology Co.), Potassium hydroxide (KOH, ⩾85 wt%, analytical purity) and nickel sulfate ($NiSO_4·6H_2O$, analytical purity), both purchased from Tianjin Bodi Chemical Co.

CHI608E electrochemical workstation (Shanghai Chen Hua Instruments Co., Ltd.), 040S ultrasonic cleaner (Shenzhen JieMeng Cleaning Equipment Co., Ltd.), DF-101Z water bath collector type constant temperature heating magnetic stirrer (Shanghai BONSI Instrument Technology Co.), 85-2 thermostatic magnetic stirrer (Shanghai Sile Instrument Co., Ltd.), FA2004 electronic balance (Changzhou Keyuan Electronic Instrument Co., Ltd.).

2.2. Electrode preparation

It consists of two main processes: pretreatment and activation preplating of the nickel substrate surface, and composite plating of nickel with hydrogen storage alloy powder.

2.2.1. Pre-treatment and pre-plating

The activated pre-plating solution was composed of $NiSO_4·6H_2O$ (240 $g·L^{-1}$), HCl (85 $mL·L^{-1}$). Before activation preplating, the working electrode was placed in acetone and sonicated for 30 min, then rinsed with deionized water and prepared for use. A two-electrode system was used for activation preplating, in which the working electrode was a 1×1 cm^2 nickel sheet and the counter electrodes are two 2 x 2 cm^2 pieces of nickel arranged on both sides of the working electrode. The working electrode was first anodically activated at a current density of 22 $mA·cm^2$ for 2 min at room temperature, and then cathodically plated with a current density of 22 $mA·cm^2$ in the reverse direction.

2.2.2. Composite plating

The base plating solution for composite plating is a modified Watt plating solution, given the concentrations of $NiSO_4·6H_2O$ (280 $g·L^{-1}$) and H_3BO_4 (40 $g·L^{-1}$), then solutions with different concentrations of hydrogen storage alloy powder (0 $g·L^{-1}$, 10 $g·L^{-1}$, 20 $g·L^{-1}$, 30 $g·L^{-1}$) are prepared, and the hydrogen storage alloy particles are uniformly dispersed in the electrolyte using 30min of ultrasonic treatment, followed by 10h of magnetic stirring. Then the plating was carried out at different temperatures (25 °C, 40 °C, 60 °C), different solution stirring rates (100 $rpm·min^{-1}$, 200 $rpm·min^{-1}$, 300 $rpm·min^{-1}$, 400 $rpm·min^{-1}$) and different deposition current densities (30 $mA·cm^{-2}$, 40 $mA·cm^{-2}$, 50 $mA·cm^{-2}$) at the same controlled power level, respectively. The composite plating also uses a two-

electrode system, and the counter electrode is the same as the pre-plating process. After electrodeposition, the samples were placed in deionized water and ultrasonically cleaned for 10 min.

2.3 Electrode characterization and performance testing

The XRD analysis was performed using an XRD-6100 X-ray diffractometer from Shimadzu, Japan, with CuKα rays, working tube voltage and tube current of 40 kV and 30 mA, respectively, and a scan rate of 2 (°)·min^{-1} with a scan range of 10° to 80°. A scanning electron microscope (SEM) SU-8010 from Hitachi, Japan, was used to observe the surface morphology of the hydrogen storage alloy powder and plating, and the composition analysis of the plating was determined by the energy spectrometer (EDS) attached to this SEM.

The electrochemical performance test was performed using the CHI608E electrochemical workstation. The test was carried out at room temperature using a three-electrode system, with a 1×1 cm^2 composite plated sample as the working electrode, two 2×2 cm^2 large area nickel sheets as counter electrodes arranged on both sides of the working electrode, Hg/HgO electrode (1M KOH) as the reference electrode, and 1M KOH as the electrolyte. The catalytic performance of the electrode for hydrogen evolution was studied by cathodic polarization test (LSV) with a scan rate of 5 mV·s^{-1} and a voltage range of -0.6 to -1.4 V (vs· Hg/HgO). The hydrogen evolution stability of the electrode was studied by constant current chrono-potentiometry (CP). The electrochemical impedance spectroscopy (EIS) of the composite electroplated electrode was tested at different bias voltages in the frequency range of 10 kHz to 0.01 Hz with an AC amplitude of 10 mV in order to have a deeper understanding of the reaction mechanism in the hydrogen evolution process.

3. RESULTS AND DISCUSSION

3.1 Effect of process parameters of composite plating on the catalytic activity of composite electrodes for hydrogen evolution

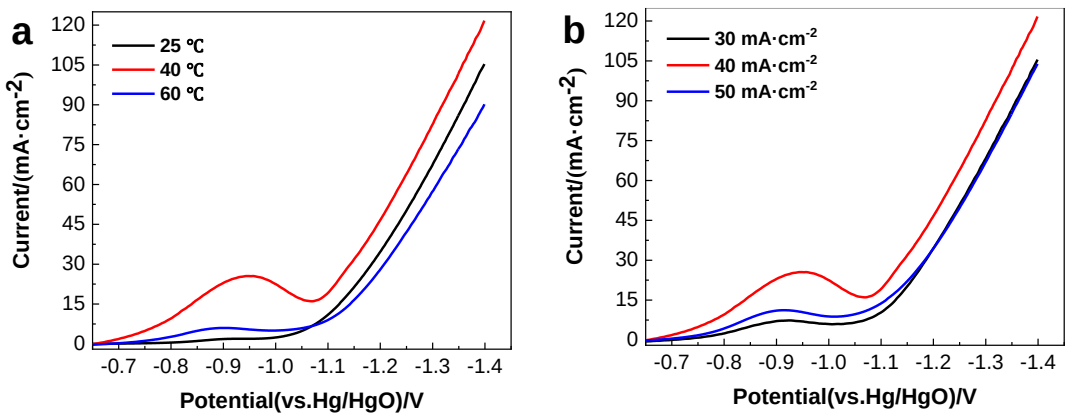

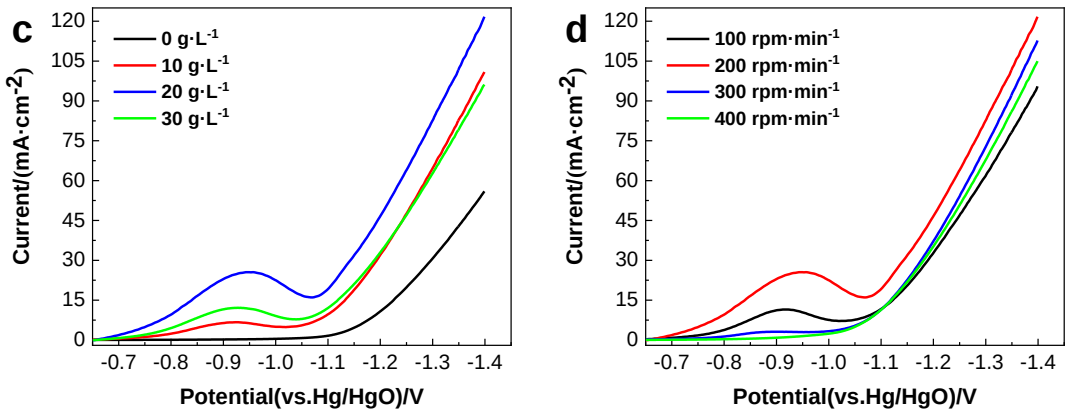

Figure 1. The cathodic polarization curves of Ni/MH composite electrode under different plating process parameters, (a) the effect of plating temperature (hydrogen storage alloy powder mass concentration 20 g·L^{-1}, solution stirring rate 200 rpm·min^{-1}, plating current density 40 mA·cm^{-2}, plating power 13.3 mA·h), (b) the effect of plating current density (hydrogen storage alloy powder mass concentration 20 g·L^{-1}, solution stirring rate 200 rpm·min^{-1}, plating current density 40 °C, plating power 13.3 mA·h), (c) the effect of the mass concentration of hydrogen storage alloy powder (solution stirring rate 200 rpm • min^{-1}, plating temperature 40 ° C, plating current density 40 mA • cm^{-2}, plating power 13.3 mA • h), (d) the effect of the solution stirring rate (Hydrogen storage alloy powder mass concentration 20 g • L^{-1}, plating temperature 40℃, plating current density 40 mA·cm^{-2}, plating power 13.3 mA·h)

The catalytic activity of hydrogen evolution of composite plating under four experimental conditions of plating temperature (25 °C, 40 °C, 60 °C), plating current density (30 mA·cm^{-2}, 40 mA·cm^{-2}, 50 mA·cm^{-2} with 13.3 mA·h), the mass concentration of hydrogen storage alloy powder (0 g·L^{-1}, 10 g·L^{-1}, 20 g·L^{-1}, 30 g·L^{-1}) and solution stirring rate (100 rpm·min^{-1}, 200 rpm·min^{-1}, 300 rpm·min^{-1}, 400 rpm·min^{-1}) were obtained using a single-factor experimental method, and the results are shown in Fig. 1. From the results, the LSV curves of all Ni/MH composite electrodes showed a reduction peak at -0.95 V (vs-Hg/HgO), where the reduction of water molecules and the adsorption of atomic hydrogen occurred [15], indicating that the hydrogen storage alloy is involved in the hydrogen evolution reaction and stores hydrogen. Fig. 1 (a) shows the LSV curves of the Ni/MH composite electrode obtained by deposition at different temperatures (hydrogen storage alloy powder mass concentration 20 g·L^{-1}, solution stirring rate 200 rpm·min^{-1}, plating current density 40 mA·cm^{-2}, plating power 13.3 mA·h), the current response at different potentials of the Ni/MH composite electrode obtained when the deposition temperature is 40 °C corresponds to higher than that of the Ni/MH composite electrode obtained at other deposition temperatures, indicating that the Ni/MH composite electrode with a deposition temperature of 40 °C has the best catalytic performance for hydrogen evolution, which is not consistent with the optimal electrodeposition temperature of Ni/LaCrO3 introduced in the literature [16], and may be related to the material of the composite deposition and the size of the particles; Fig. 1 (b) shows the LSV curves of the Ni/MH composite electrode obtained by plating at different plating current densities (mass concentration of hydrogen storage alloy powder 20 g·L^{-1}, solution stirring rate 200 rpm·min^{-1}, plating temperature 40 °C, plating power 13.3 mA·h), the Ni/MH composite electrode obtained at a deposition current density of 40 mA·cm^{-2} exhibited the best catalytic performance for hydrogen evolution, while the deposition

current densities of 30 mA·cm^{-2} and 50 mA·cm^{-2} showed comparable catalytic performance for hydrogen evolution; Fig. 1 (c) shows the LSV curves of Ni/MH composite electrodes obtained by plating at different mass concentrations of hydrogen storage alloy powder (solution stirring rate 200 rpm·min^{-1}, plating temperature 40 °C, plating current density 40 mA·cm^{-2}, plating power 13.3 mA·h), the best hydrogen evolution catalytic performance of the Ni/MH composite electrode obtained by electrodeposition was achieved at a mass concentration of hydrogen storage alloy powder of 20 g·L^{-1}. This may be due to the fact that the deposition of hydrogen storage alloy powder during electroplating at this mass concentration can well match the deposition of nickel and create a larger specific surface area for nickel deposition [17]; Fig. 1 (d) shows the LSV curves of Ni/MH composite electrode obtained by plating at different solution stirring rates (mass concentration of hydrogen storage alloy powder 20 g·L^{-1}, plating temperature 40°C, plating current density 40 mA·cm^{-2}, plating power 13.3 mA·h), the best catalytic performance of hydrogen evolution corresponding to Ni/MH composite plating was achieved at 200 rpm·min^{-1}. Too low a rotation speed would reveal that many alloy particles at the bottom of the vessel were not dispersed in the solution, while too high a rotation speed would be detrimental to the bonding of the alloy particles to the substrate and thus to the subsequent deposition process.

In summary, the optimal composite plating conditions were obtained using the single-factor experimental method as follows: plating temperature of 40 °C, plating current density of 40 mA·cm^{-2} (power 13.3 mA·h), the mass concentration of hydrogen storage alloy of 20 g·L^{-1}, and solution stirring rate of 200 rpm·min^{-1}. The Ni/MH composite electrode prepared under the optimal composite plating conditions has good catalytic activity, and the electrode prepared under the optimal conditions will be investigated in more depth at the hydrogen evolution and structural levels in order to further obtain the reasons for the superior catalytic performance of the composite plated Ni/MH hydrogen evolution.

3.2 Physical phase analysis and morphological characterization of the plated layer

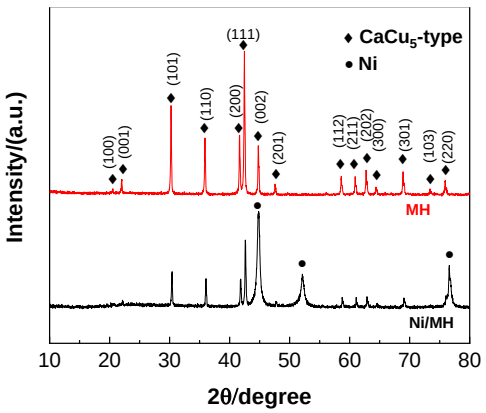

Figure 2. XRD patterns of commercially available MH powder and electroplated Ni/MH electrode

XRD patterns of the commercially available hydrogen storage alloy powder (MH) and the composite electroplated plating (Ni/MH electrode) under optimal process conditions are shown in Fig. 2. As seen in Fig. 2, the XRD curve of the upper hydrogen storage alloy powder retains the typical

$CaCu_5$-type hexagonal structure [18, 19], and the peak shape and crystal plane also match, which indicates that the experimental procedure in this paper does not affect the crystal structure of the alloy. The lower curve corresponds to the XRD pattern of the Ni/MH electrode of the composite electroplated layer, and it can be seen that there are $CaCu_5$-type diffraction peaks on the curve with the same position of the hydrogen storage alloy powder above, which indicates that there is an obvious hydrogen storage alloy powder in the composite plating. In addition, the XRD curves of Ni/MH electrode showed strong diffraction peaks of Ni at 2θ=44.60°, 51.98°, 76.59°, which were tentatively judged to belong to Ni plating in composite plating, and the following will be combined with SEM and EDS results for detailed analysis.

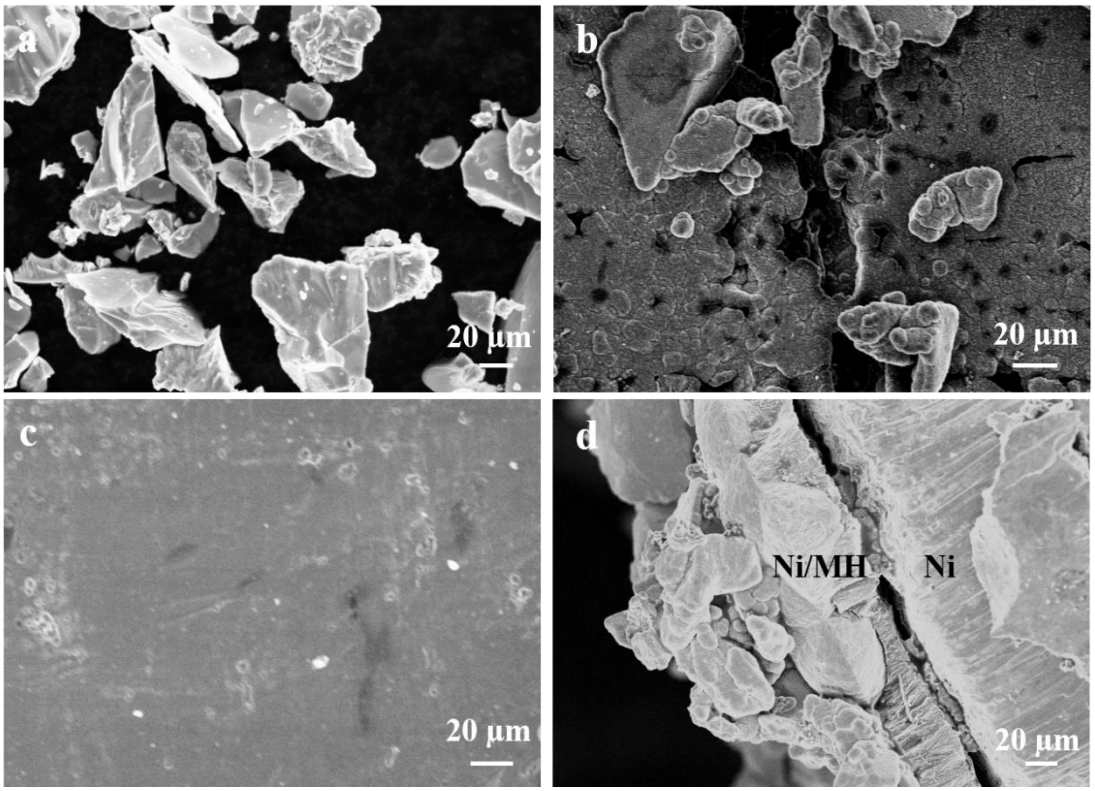

Figure 3. SEM images of different samples, (a) MH powder, (b) Ni/MH composite coating surface, (c) Nickel foil substrate surface, (d) Ni/MH composite coating section

The SEM images of different samples are shown in Fig. 3, where Fig. 3 (a) shows the commercial MH hydrogen storage alloy powder with particles as large as about 80 μm and as small as a few μm, with an average particle size of about 50 μm, as described by the manufacturer. Fig. 3 (b) shows the composite plated Ni/MH electrode prepared under the optimal process conditions, where it can be clearly seen that the plated surface is embedded with hydrogen storage alloy powder particles, and there are many holes of different sizes on the surface of the Ni plating, which increases the specific surface area of the electrode. Fig. 3 (c) shows the surface of the flat nickel foil substrate, and it can be seen that the substrate surface was very smooth before the composite plating was applied. Fig. 3 (d) is a cross-section of the composite plating obtained using the physical cutting method, and it can be seen that there are

particles embedded in the plating, not only on the surface of the plating shown in Fig. 3 (b), and in turn, it can be speculated that the porosity presented on the surface of the plating in Fig. 3 (b) may be caused by the hydrogen storage alloy powder during the deposition process.

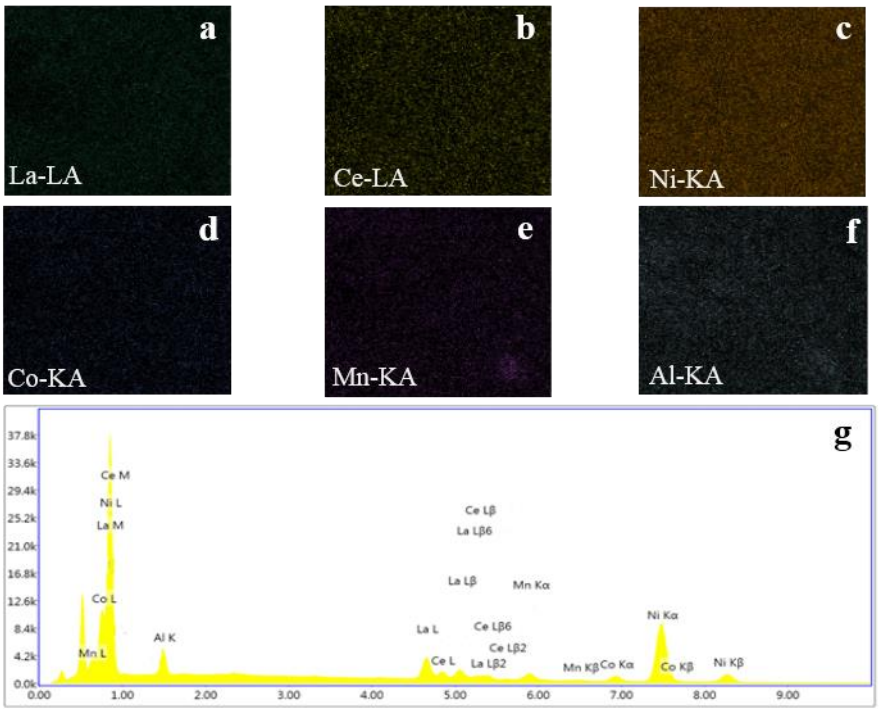

Figure 4. EDS element map of (a) La, (b)Ce, (c)Ni, (d)Co, (e)Mn, (f)Al and (g) EDS spectrum of Ni/MH composite coating

Table 1. The chemical composition of the composite coating measured by EDS

Element		La	Ce	Ni	Co	Mn	Al
Weight%	composite coating	9.53	3.94	64.59	6.67	5.85	9.42
Atomic%	composite coating	6.29	2.45	72.93	4.54	3.67	10.13

Table 2. Element mass ratio of $MmNi_{4.05}Co_{0.45}Mn_{0.38}Al_{0.3}$ alloy powder

Element	Mm	Ni	Co	Mn	Al
Weight%	32.2±1.0	55.0±1.0	6.1±0.5	4.8±0.5	1.9±0.5

The EDS spectra of the composite plated Ni/MH electrode prepared under the optimal process conditions were tested with a scanning electron microscope self-contained energy spectrum analyzer, and the surface distribution and intensity analysis of different elements are shown in Fig. 4. From the face-scan elemental mapping of Ni/MH of composite plating Fig. 4 (a)-(f), it can be seen that La, Ce, Ni, Co, Mn and Al are basically uniformly distributed in the alloy, which indicates that the plating contains MH powder particles and is dispersed and buried by the nickel plating. The EDS spectra are

shown in Fig. 4 (g), and the chemical composition ratios are shown in Table 1. Provided in Table 2 are the mass ratios of the elements of $MmNi_{4.05}Co_{0.45}Mn_{0.38}Al_{0.3}$ alloy powder provided by the merchant. It can be seen that after composite plating, the content of four elements Ni, Co, Mn and Al increased and the content of La and Ce decreased. The increase of Ni content should be related to the Ni plating of the composite plating, and the change of the content of other elements may be related to the erosion of the composite plating solution, as shown in the literature [19], which showed that the elemental content of the alloy changed after treatment in the solution.

3.3 Comparison of electrochemical properties of different electrodes

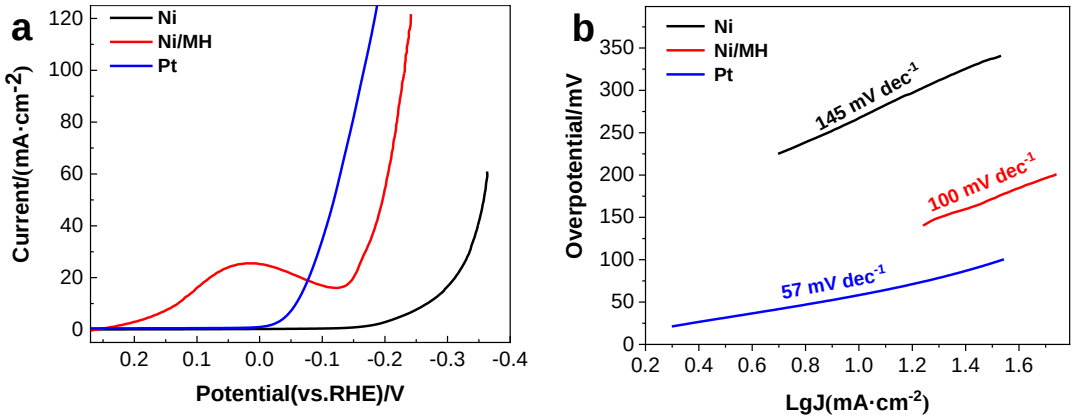

Figure 5. Plots of (a) polarization curves and (b) tafel curves for different electrodes

The cathodic polarization curves (which have been converted to reversible hydrogen potential) and the intercepted η-logj relationship (Tafel relationship) curves of the hydrogen evolution polarization region for the three electrodes, Ni foil, Ni/MH (composite coating under optimal process conditions) and Pt, are shown in Fig. 5. The corresponding Tafel slope can be obtained according to the Tafel relation (1) [20]:

$$\eta = b\log j + a \quad (1)$$

where j is the current density, a is the overpotential at j = 1A·cm^{-2}, b is the Tafel slope, and η is the overpotential.

The final displayed hydrogen evolution potential is the value relative to the reversible hydrogen electrode (RHE) after eliminating the effect of solution resistance [21], which can be obtained from Equation (2) [22]:

$$E(RHE) = E(Hg/HgO) + 0.098V + 0.059 \times pH \quad (2)$$

Using Ni and Pt electrodes as controls, Fig. 5 (a) shows that the Ni/MH composite electrode has good catalytic performance for hydrogen evolution, with a reduction peak near the overpotential 0 V for the hydrogen absorption phase of the hydrogen storage alloy and high current response, as already mentioned in Fig. 1 to study the catalytic performance of the electrode under different preparation conditions. The overpotential of Ni/MH composite electrode is 196 mV when the current density reaches 50 mA·cm^{-2} and 231 mV when the current density reaches 100 mA·cm^{-2}. Although the Ni electrode has good hydrogen evolution performance in alkaline solution, it still has many gaps compared with the

Ni/MH composite electrode. The Pt electrode has the best hydrogen evolution performance among the three electrodes, and the starting potential of hydrogen evolution is the lowest, close to 0 V. The corresponding overpotential is 118 mV at a current density of 50 mA·cm^{-2} and 166 mV at a current density of 100 mA·cm^{-2}. Fig. 5(b) shows the Tafel curve transformed from Fig. 5(a), and the Tafel slope of the fitted linear part best visualizes the evolutionary route of hydrogen from the hydrogen evolution process [23], where the Ni/MH composite electrode described in this paper has a Tafel slope of 100 mV·dec^{-1}, which is smaller than the Ni-Co-LaNi$_5$ electrode Tafel slope described in the literature [24].

3.4 Electrode hydrogen evolution stability test

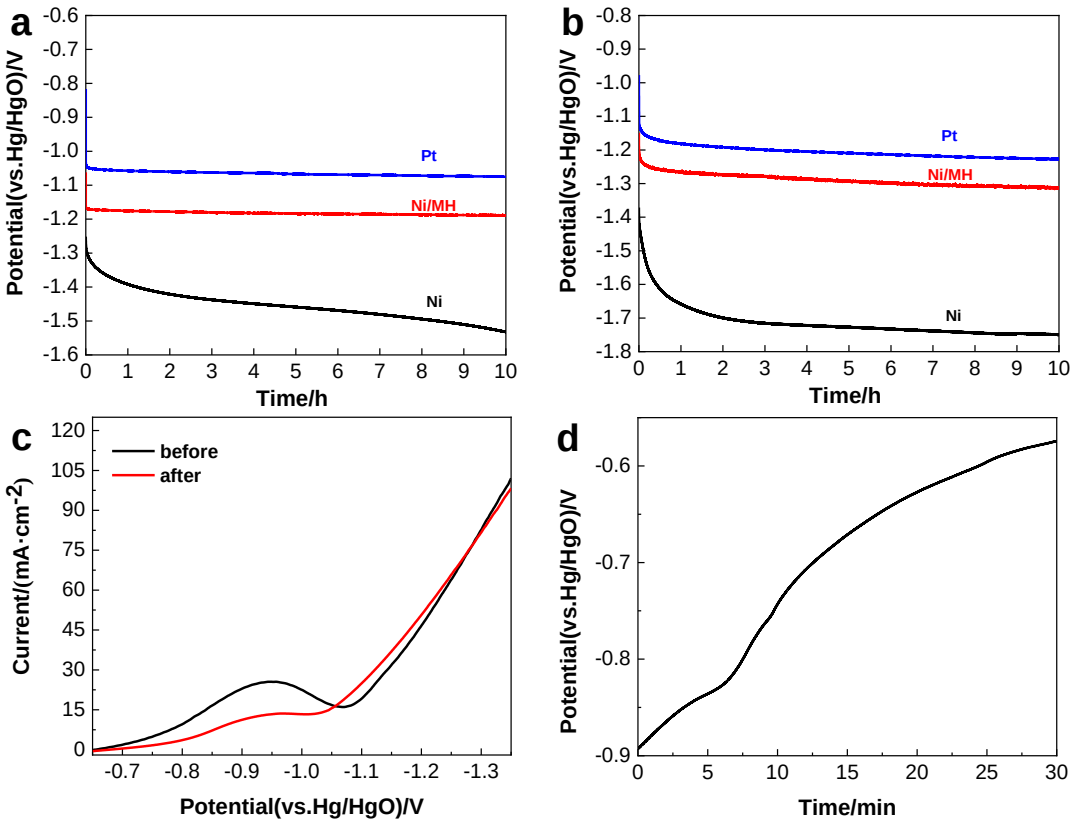

Figure 6. Test chart of hydrogen evolution stability of composite electrode, (a) potential-time curve at 20mA·cm^{-2} (Ni, Ni/MH and Pt electrodes), (b) potential-time curve at 50mA·cm^{-2} (Ni, Ni/MH and Pt electrodes), (c) comparison of LSV curves of Ni/MH composite electrodes before and after hydrogen evolution at 20 mA·cm^{-2} for 10 hours, (d) open circuit potential (OCP)-time curve of Ni/MH composite electrode after hydrogen evolution at 20mA·cm^{-2} for 10 hours

In the practical application of hydrogen evolution electrode, stability is an important index, and the stability of the electrode can be visualized by applying a constant current density to the working electrode for a long time and recording its potential response at the same time. The potential-time curves of Ni, Ni/MH and Pt electrodes were tested at different current densities, as shown in Fig. 6(a) for the potential-time curve at 20 mA·cm^{-2} and in Fig. 6(b) for the potential-time curve at 50 mA·cm^{-2}. It can be seen that the potential response of Ni/MH composite electrode is very stable at a current density of

20 mA·cm^{-2}; the potential of Ni/MH composite electrode decreases slightly with time at a current density of 50 mA·cm^{-2}. The potential of Ni electrode decreases all the time at either 20 mA·cm^{-2} or 50 mA·cm^{-2}, indicating that the Ni electrode is less stable for hydrogen analysis. hydrogen separation stability is poor. The potential drop of Pt electrode is not obvious at 20 mA·cm^{-2} current density, but at high overpotential 50 mA·cm^{-2} current density it can be clearly seen that the potential is also slowly decreasing with the increase of time. Overall, the stability of Ni/MH composite electrode can be comparable to or even better than that of Pt electrode.

Fig. 6(c) shows the comparison of LSV curves of Ni/MH composite electrode before and after 10h of hydrogen evolution at 20mA·cm^{-2}. It can be found that the reduction peak of LSV curves measured after the constant current test is greatly weakened, but the hydrogen evolution performance at high overpotential does not change; at low overpotential, the hydrogen evolution performance of Ni/MH composite electrode becomes slightly better after 10h of hydrogen evolution. The two hydrogen evolution polarization curves near -1.3 V (vs. Hg/HgO) almost overlap, indicating that the Ni/MH composite electrode has good hydrogen evolution stability. The reason for the weakening of the reduction peak of the Ni/MH composite electrode after 10 h of hydrogen evolution is supposed to be that the hydrogen adsorbed by the energy storage alloy in the plating has almost reached saturation due to the long hydrogen evolution process [25].

Fig. 6(d) shows the curve of Ni/MH composite electrode open circuit potential (OCP) with time after hydrogen evolution at 20 mA·cm^{-2} for 10 h. The test time is half an hour, and the open circuit potential of Ni/MH composite electrode moves in the positive direction with the increase of time, about 7 min before the open circuit Ni/MH composite electrode potential moves more slowly, which should correspond to the electrochemical release of hydrogen absorbed by the energy storage alloy. The accelerated positive shift of Ni/MH composite electrode potential after about 7 min of open circuit (obvious inflection point), which should be the exhaustion of hydrogen absorbed by the energy storage alloy. The stable open-circuit potential of the Ni/MH composite electrode before electrolysis was about -0.37 V (vs·Hg/HgO), while 30 min after the electrolysis measurement of the open-circuit potential, the potential of this electrode was still at -0.43 V (vs·Hg/HgO), which is more negative than before electrolysis, which is consistent with the phenomenon shown in Fig. 6(c). In addition, the absorption of a large amount of hydrogen by the hydrogen storage alloy prevents the electrode from being oxidized in case of power failure, i.e., it is resistant to power failure [11], thus providing electrochemical protection for this electrode.

3.5 Electrochemical impedance spectroscopy

Fig. 7(a) shows the electrochemical impedance spectra of nickel foil electrode (Ni), nickel-based nickel-plated electrode (Ni@Ni, hydrogen storage alloy powder mass concentration 0 g·L^{-1}, solution stirring rate 200 rpm • min^{-1}, plating temperature 40 ° C, plating current density 40 mA • cm^{-2}, plating power 13.3 mA • h) and composite electrode (Ni/MH) at an overpotential of 200 mV at room temperature, and Fig. 7(b) shows the equivalent circuit diagrams fitted to the three electrodes under this condition, and the values of the parameters obtained from the fitting are shown in Table 3, where R_s is

the solution resistance, R_{ct} is the charge transfer resistance, and C_{dl} is the bilayer capacitance of the electrode surface [24, 26].

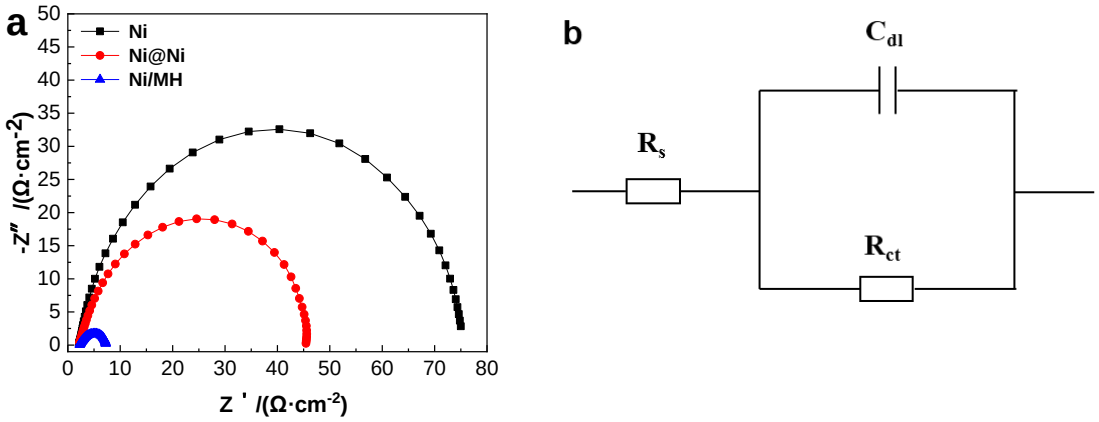

Figure 7. Plots of (a) electrochemical impedance spectra and (b) equivalent circuits for different electrodes

Table 3. Fitting parameters of equivalent circuit of different electrodes under 200mV overpotential

Electrode	R_s/(Ω·cm^{-2})	C_{dl}/(μF·cm^{-2})	R_{ct}/(Ω·cm^{-2})	j^0/(A·cm^{-2})
Ni	2.483	101.4	76.53	1.678×10^{-4}
Ni@Ni	2.382	123.6	42.56	3.017×10^{-4}
Ni/MH	2.538	1002	4.717	2.722×10^{-3}

The impedance spectra of all three electrodes exhibit a single circular arc as seen in the figure, indicating that all three electrodes are electrochemically controlled processes under this condition; the Ni/MH composite electrode impedance has the smallest semicircle, indicating that this electrode has a small charge transfer resistance and possesses good charge transfer capability. The Ni@Ni electrode impedance has the middle arc radius and the Ni electrode impedance has the largest arc radius. The apparent exchange current density j^0 of the three electrodes at the given overpotential can be obtained according to Eq. (3) (listed in Table 3):

$$j^0 = \frac{RT}{nFR_{ct}} \quad (3)$$

In the formula: R is the gas constant, T is the absolute temperature, F is the Faraday constant, n is the number of reaction electrons. As seen from the data in Table 3, the apparent exchange current densities of Ni/MH composite electrode, Ni@Ni electrode, and Ni electrode were 2.72×10^{-3}A·cm^{-2}, 3.02×10^{-4}A·cm^{-2}, and 1.68×10^{-4}A·cm^{-2}, and the adsorption capacitances of the three electrodes are 1002μF·cm^{-2}, 123.6μF·cm^{-2}, and 101.4μF·cm^{-2}, respectively. The Ni/MH composite electrode has the highest exchange current density at the corresponding overpotential, the apparent exchange current density of Ni/MH composite electrode is 16.21 times and 9.017 times that of Ni@Ni electrode and Ni electrode, which indicates that the Ni/MH composite electrode has the fastest electrode reaction rate and the best electrochemical activity. The apparent specific surface area of the Ni/MH composite electrode

can be approximated from the value of the bilayer capacitance Cdl to be 50.13 cm^2 [27], which is 8.1 times and 9.9 times of Ni@Ni electrode and Ni electrode, respectively. It can be assumed that the best catalytic activity of Ni/MH composite electrode among the three is not only related to its highest specific surface area, but also to the improved electrochemical reactivity (apparent exchange current density) of Ni/MH composite electrode.

3.6 Mechanism of hydrogen evolution activity of Ni/MH composite electrode

The alkaline HER process usually involves three reaction mechanisms (Eqs. (4)-(6), M is the catalytic electrode surface active point):

$$H_2O+M+e^-\rightarrow M\text{-}H+OH^- \text{ (Volmer reaction)} \quad (4)$$

$$H_2O+e^-+M\text{-}H\rightarrow M+H^2+OH^- \text{ (Heyrovsky reaction)} \quad (5)$$

$$M\text{-}H+M\text{-}H\rightarrow 2M+H^2 \text{ (Tafel reaction)} \quad (6)$$

A water molecule is electrochemically reduced on the electrode surface and produces an adsorbed hydrogen atom (Volmer reaction), another water molecule is then electrochemically reduced on the electrode surface and produces a hydrogen molecule (Heyrovsky reaction), or a combination of two adsorbed hydrogen atoms on the electrode surface produces a hydrogen molecule (Tafel reaction). Based on the Tafel slope values of the Ni/MH composite electrode at room temperature shown in Figure 5(b), it can be deduced that the hydrogen evolution mechanism is mainly Eq. (4) and Eq. (6) [20], where water molecules reach the electrode surface and undergo electrochemical reduction to generate adsorbed hydrogen (Eq. (4) Volmer reaction), and two adsorbed hydrogens combine to form hydrogen molecules (Eq. (6) Tafel reaction). For HER, the H_2O-M bond should be strong enough to facilitate the splitting of water molecules; on the contrary, the H-M bond should not be too strong to facilitate the evolution of H^2. Since the adsorption of H_2O molecules and the decomposition of water molecules after adsorption (H-O bond breaking) require a large amount of energy, it can be inferred that the adsorption step in the Volmer reaction is a rate control step (RDS). During the Volmer reaction, the discharge of H_2O molecules requires paired d-orbital electrons, such as those of Ni, which facilitate the transfer of electrons to H_2O molecules and promote the cleavage of O-H bonds and the subsequent formation of M-H bonds. Subsequently, the electrode surface needs to have half-empty d orbitals, such as those of La, Ce, Co, and Mn [20, 28], which facilitate H adsorption. It can be seen that $MmNi_{4.05}Co_{0.45}Mn_{0.38}Al_{0.3}$ hydrogen storage alloy powder enhances the H adsorption on the electrode surface, and the synergistic effect with Ni metal elements makes the Ni/MH composite electrode have high catalytic activity for hydrogen evolution.

4. CONCLUSIONS

In this paper, the best process conditions to composite electroplated Ni/MH electrode under the listed conditions were screened out by the method of single-factor experiments with the cathodic polarization curve of the electrode as the index, and then the catalytic performance of the electrode for

hydrogen evolution was investigated more deeply by using characterization and electrochemistry, and the following conclusions were obtained:

1. The peak types of the composite plating tested by XRD are the diffraction peak of Ni and the $CaCu_5$ type (AB_5 type) diffraction peak retained by the hydrogen storage alloy powder.

2. SEM testing revealed the presence of alloy particles on the surface of the plating, as well as inlaid alloy particles inside the plating, and EDS testing of the plating also showed that the plating contained elements contained in the alloy powder.

3. The Ni/MH electrode was obtained by composite plating, and the corresponding overpotential was 231 mV with a Tafel slope of 100 $mV \cdot dec^{-1}$ at a current density of 100 $mA \cdot cm^{-2}$, indicating good catalytic performance. Stability tests also showed that the electrode has good stability for hydrogen evolution. The electrochemical impedance test showed that the electrode has good charge transfer resistance and has a high specific surface area. $MmNi_{4.05}Co_{0.45}Mn_{0.38}Al_{0.3}$ hydrogen storage alloy powder enhances the H adsorption on the electrode surface, and the synergistic effect with Ni metal elements makes the Ni/MH composite electrode have a high catalytic activity of hydrogen evolution.

In summary, $MmNi_{4.05}Co_{0.45}Mn_{0.38}Al_{0.3}$ hydrogen storage alloy powder can be used as a catalyst for hydrogen evolution, and it is cheap compared with precious metals, has high catalytic performance and stability, and can be used for both hydrogen storage and hydrogen evolution applications.

References

1. C.-J. Winter, *International journal of hydrogen energy*, 34(2009)S1-S52.
2. T. N. Veziroğlu and S. Şahi, *Energy conversion and management*, 49(2008)1820-1831.
3. S. Dutta, *International Journal of Hydrogen Energy*, 15(1990)379-386.
4. P. C. K. Vesborg, B. Seger and I. Chorkendorff, *Journal of Physical Chemistry Letters*, 6(2015)951-957.
5. I. A. Raj and K. I. Vasu, *Journal of Applied Electrochemistry*, 20(1990)32-38.
6. I. A. Raj and K. I. Vasu, *Journal of Applied Electrochemistry*, 22(1992)471-477.
7. S.-Z. Yang, C.-H. Gao and N. LI, *Metallic Functional Materials*, 1(2008)36-39.
8. H. Van Mal, K. Buschow and A. Miedema, *Journal of the Less Common Metals*, 35(1974)65-76.
9. Z. Yi, W. Senlin and L. Caicai, *Rare Metal Materials and Engineering*, 3(2012)457-461.
10. Q.-S. Song, Z.-Y. Tang, H.-T. Guo and S. Chan, *Tianjin Daxue Xuebao(Journal of Tianjin University of Science and Technology)*, 38(2005)508-512.
11. H. Qing, C. Jianshe, L. Kuiren and W. Xujun, *Acta Metallurgica Sinica*, 44(2008)887-891.
12. T. Kitamura, C. Iwakura and H. Tamura, *Electrochimica Acta*, 27(1982)1723-1727.
13. C. Briki, P. de Rango, S. Belkhiria, M. H. Dhaou and A. Jemni, *International Journal of Hydrogen Energy*, 44(2019)13647-13654.
14. J. Liu, K. Li, H. Cheng, K. Yan and Z. Zheng, *International Journal of Hydrogen Energy*, 42 (2017) 24904-24914.
15. D. Q.-H. W. Sen-Lin and W. Li-Pin, *Acta Physico-Chimica Sinica*, 1(2013)123-130.
16. N. Shaigan, D. G. Ivey and W. Chen, *Journal of the Electrochemical Society*, 155(2008)D278.
17. Y. Wei, Y. U. Zhi-Yong, L. I. Xin-Jie, G. Shi-Wang, L. Lian-Bo and S. Jun-Jie, *Electroplating & Finishing*, 7(2017)337-341.
18. R. Cui, C. Yang, M. Li, B. Jin, X. Ding and Q. Jiang, *Journal of Alloys and Compounds*, 693(2017)126-131.
19. G. Su, Y.-h. He and K.-y. Liu, I*nternational journal of hydrogen energy*, 37(2012)12384-12392.

20. L. Wu, X. Guo, Y. Xu, Y. Xiao, J. Qian, Y. Xu, Z. Guan, Y. He and Y. Zeng, *RSC advances*, 7(2017)32264-32274.
21. J. Zhao, X. Ren, Q. Han, D. Fan, X. Sun, X. Kuang,Q. Wei and D. Wu, *Chemical Communications*, 54(2018) 4987-4990.
22. A. Kellenberger, N. Vaszilcsin, W. Brandl and N. Duteanu, *International Journal of Hydrogen Energy*, 32(2007)3258-3265.
23. R. D. Nikam, A. Y. Lu, P. A. Sonawane, U. R. Kumar, K. Yadav, L. J. Li and Y. T. Chen, *ACS Appl Mater Interfaces*, 7(2015)23328-23335.
24. G. Wu, N. Li, C. S. Dai and D. R. Zhou, *Materials Chemistry and Physics*, 83(2004)307-314.
25. Chen, W., Z. Tang, and H. Guo, *Chinese Journal of Power Sources*, 22(1998)115-118.
26. A. R. Madram, M. Mohebbi, M. Nasiri and M. R. Sovizi, *Iranian Journal of Hydrogen & Fuel Cell*, 5(2018)1-11.
27. M. Metikoš-Huković and A. Jukić, *Electrochimica acta*, 45(2000)4159-4170.
28. Z. Chen, G. Shao, Z. Ma, J. Song, G. Wang and W. Huang, *Materials Letters*, 160(2015)34-37.